Paleozoic carbonate-hosted deposits of the southern Rocky Mountains: a review

Paradis, S.[1*], Simandl, G.J.[2], Drage, N.[3], D'Souza, R.J.[2], Kontak, D.J.[4], Waller, Z.[4]

[1]Geological Survey of Canada, Sidney, BC
[2]British Columbia Geological Survey, Victoria, BC
[3]Dalhousie University, NS
[4]Laurentian University, ON
*corresponding author: suzanne.paradis@canada.ca

Recommended citation:
Paradis, S., Simandl, G.J., Drage, N., D'Souza, R.J., Kontak, D.J., and Waller, Z., 2020. Paleozoic carbonate-hosted deposits of the southern Rocky Mountains: a review. British Columbia Ministry of Energy, Mines and Petroleum Resources, British Columbia Geological Survey GeoFile 2020-07.

Natural Resources Canada / Ressources Naturelles Canada

British Columbia — Ministry of Energy, Mines and Petroleum Resources

Abstract, location, and stratigraphy

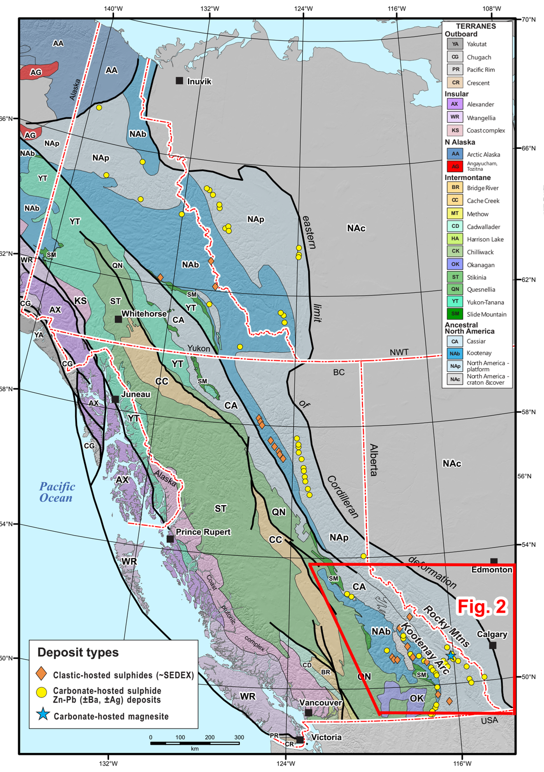

Figure 1. Terranes of the Canadian Cordillera [1] and location of sediment-hosted deposits in rocks of the Ancestral North America margin.

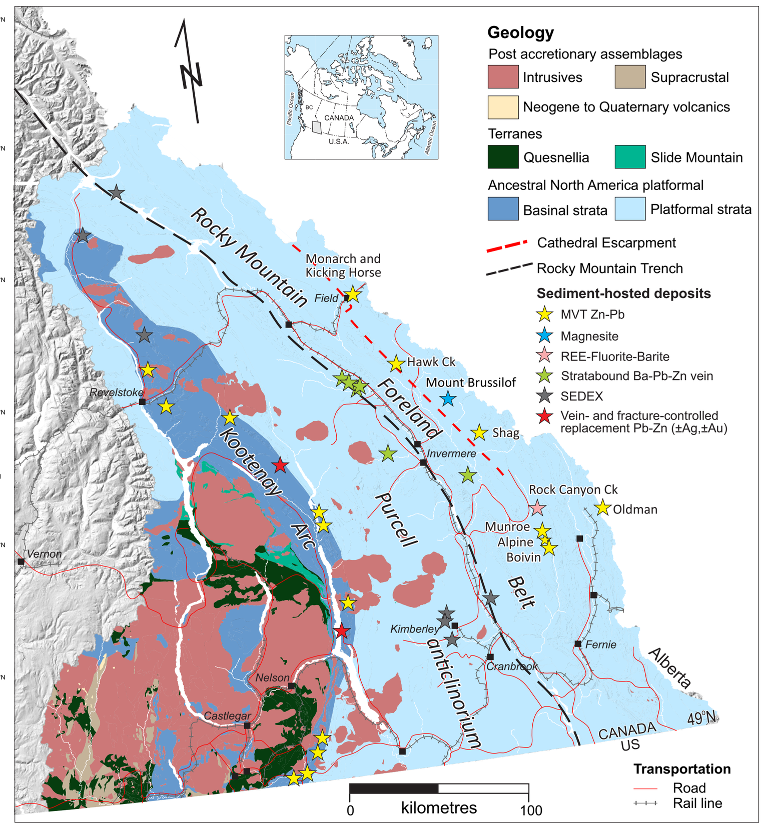

Figure 2. Regional geological map of southeastern Canadian Cordillera showing locations of the sediment-hosted deposits. The projection of the Cathedral escarpment (red dashed-line) corresponds approximately to the western margin location of the Kicking Horse Rim, a paleogeographic high that was initiated in the early middle Cambrian and persisted into the Ordovician [2,3]. Both features mark the change from shallow-water carbonate rocks to the east and continental slope lithofacies to the west during the early Paleozoic. Modified from [4]. Terranes from [5].

Abstract

The Paleozoic carbonate rocks of the southeastern Canadian Cordillera contain a variety of deposit types, including Mississippi Valley-type, magnesite, and REE-F-Ba. These deposits are hosted in weakly deformed, and metamorphosed Paleozoic platform carbonate rocks of the Rocky Mountains. They are found at different stratigraphic levels, however, most of them are hosted in dolostones of the middle Cambrian Cathedral Formation, upper Cambrian Jubilee Formation and Upper Devonian Palliser Formation.

The deposits occur along major structurally controlled facies transitions between the shallow-water carbonate platforms and deeper water basin rocks of the Paleozoic continental margin. The location and geometry of these deposits reflect the juxtaposition of structures (e.g., deep-seated faults at platform to deep-water basin transition) and rock types (i.e., permeable and reactive stratigraphic units) favorable to mineralization. This confluence of favorable conditions resulted from episodic rifting and mineralization along the Paleozoic margin during the middle to Late Cambrian and Late Devonian to Middle Carboniferous.

This poster reviews geology, petrography, stable (C, O, S) and radiogenic (Pb, Sr) isotopes, and geochronology of selected carbonate-hosted deposits. Petrography shows dissolution and replacement of the original carbonate by fine-grained "dolomite" followed by different stages of coarser dolomite replacement and cavity fracture fillings (e.g., saccharoidal, sparry and saddle dolomites) accompanied by sulphide deposition, mainly sphalerite, galena and pyrite. Geochemical signatures for each mineralization type show a pattern of dolomitizing and mineralizing fluids interacting with barren host rocks. A more detailed account of the materials presented here can be found in [6].

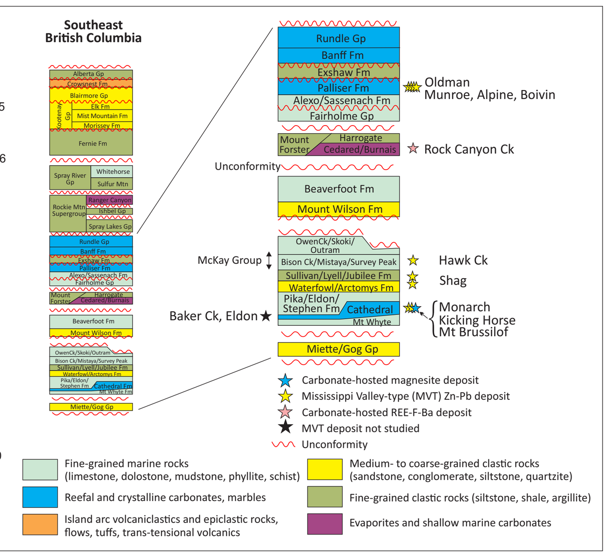

Figure 3. Generalized stratigraphy of the Purcell anticlinorium and the Rocky Mountain Foreland Belt with locations of studied deposits indicated by stars. Modified from [4].

Geology

The carbonate-hosted deposits discussed in this poster are in the southern Rocky Mountain Foreland Belt (RMFB; **Figs. 1, 2**), which is a thin-skinned thrust-and-fold belt that developed along a basal-detachment fault system initiated by Late Jurassic to Paleogene eastward accretion of allochthonous terranes [7, 8]. The strata within the RMFB consist of late Neoproterozoic to Mid-Jurassic imbricated and folded predominantly sedimentary rocks deposited on or adjacent to the stable craton of the Cordilleran margin of ancestral North America.

The strata include:

- Neoproterozoic to lower Cambrian siliclastic rocks of the Windermere Supergroup deposited during intracontinental rifting.
- Cambrian to Jurassic platform to deep-water basin transition sequences deposited on and near the ancient continental margin of ancestral North America. The Kicking Horse Rim, which corresponds approximately to the projection of the Cathedral escarpment and other escarpments, is an important Paleozoic fault-controlled, paleogeographic high at the platform to basin facies transition.
- Late Jurassic to early Cenozoic marine to non-marine siliclastic rocks eroded from the uplifting Omineca and Foreland belts.

Several carbonate-hosted deposits occur along the platform to deep-water basin transition. For example, east of the projected western margin of the Kicking Horse Rim and the Cathedral Escarpment, middle to upper Cambrian, Ordovician, and Upper Devonian shallow-water platform carbonate rocks host Mississippi Valley-type (MVT; e.g. Monarch and Kicking Horse, Boivin−Munroe−Alpine, Shag, Hawk Creek, and Oldman), magnesite (e.g. Mount Brussilof), and rare-earth element (REE)–F-Ba (e.g. Rock Canyon Creek) deposits (**Figs. 2, 3; Table 1**). West of the Kicking Horse Rim and Cathedral Escarpment, deep-water basin rocks of the Chancellor Group include the Burgess Shale Formation, and lesser accumulations of limestone and lenses of MgO- and Ba-rich chloritic rocks.

Geology

Rocky Mountains Carbonate-hosted Deposits

The Paleozoic carbonate rocks of the southeastern Canadian Cordillera contain a variety of deposit types, including MVT, REE-F-Ba, and sparry magnesite. The deposits are at different stratigraphic levels, however, most of them are hosted in dolostones of the middle Cambrian Cathedral, upper Cambrian Jubilee, and Upper Devonian Palliser formations (**Fig. 3**). Most of them occur along major structurally controlled facies transitions between the shallow-water carbonate platforms and deep-water basin rocks near the shelf-slope break of the Paleozoic continental margin. The location and geometry of these deposits reflect the association of structures (e.g. deep-seated faults at platform to deep-water basin transition) and rock types (i.e. permeable and reactive stratigraphic units) favorable to mineralization.

Mississippi Valley-type (MVT) deposits consist of stratabound lenses, layers, pods, breccias, and veins of sulphides preferentially hosted in dolostone of the middle Cambrian Cathedral and Upper Devonian Palliser formations.
Examples: Monarch and Kicking Horse, Munroe, Shag, and Boivin (**Figs. 4, 5, 6, 7, 8**).
Orebodies have single or multiple lenses in dolomitized and/or siliceous carbonate rocks. They are at facies transitions between shallow-water carbonate platform and deeper basin rocks and major basement-controlled structures.
Sulphides: Pyrite, sphalerite, galena, and minor chalcopyrite.
Gangue: Dolomite, fluorite, calcite, quartz, and minor barite.

Magnesite deposits are preferentially hosted in middle Cambrian shallow marine carbonate rocks of the Cathedral Formation. Magnesite textures vary widely.
Example: Mount Brussilof; producing mine (**Fig. 9**).
Orebodies are stratbound layers, lenses, pods and irregular masses of white to grey magnesite hosted in fine-grained dolostone.
Mineralization: Magnesite.
Main gangue minerals: Dolomite, calcite, pyrite, quartz, and clay.
Minor to trace minerals: mica, Mg-rich chlorite, talc, palygorskite/attapulgite, boulangerite, chalcocite, huntite, brucite, fersmite, Nb-bearing rutile, goyazite, and euclase.

Rock Canyon Creek REE-F-Ba deposit is hosted by dolostone, dolomitic limestone, and carbonate breccia of the Middle Devonian Cedared and Burnais formations (known to contain silty calcareous gypsum).
Orebody is steeply dipping and coincides with a crackle breccia in carbonate rocks.
Mineralization (**Fig. 10**): REE-F-Ba in REE-bearing fluorocarbonates [bastnaesite-(Ce), parisite-(Ce), synchysite-(Ce)] and a mixture of REE phosphates including monazite-(Ce).
Gangue: Dolomite, pyrite, barite, calcite, quartz, and k-feldspar.

Table 1. Principal characteristics of carbonate-hosted deposits of southeastern British Columbia invesitaged during this study

Deposit	Deposit Classification	Commodity	Formation / Unit	Age of Host Rocks	Lithology	Mineralogy
Mount Brussilof	Magnesite	Magnesite	Cathedral Fm	Middle Cambrian	Magnesite	Magnesite. Main gangue minerals: dolomite, calcite, pyrite, quartz, and clay. Minor to trace minerals: mica, Mg-rich chlorite, talc, palygorskite/attapulgite, boulangerite, chalcocite, huntite, brucite, fersmite, Nb-bearing rutile, goyazite, and euclase.
Monarch	MVT	Zn, Pb (±Ag, ±Cd)	Cathedral Fm	Middle Cambrian	Massive to thin-bedded brecciated dolostone	Galena, sphalerite and pyrite in gangue of dolomite and calcite. Minor chalcopyrite, barite, quartz and native silver.
Kicking Horse	MVT	Zn, Pb (±Ag, ±Cd)	Cathedral Fm	Middle Cambrian	Massive to thin-bedded brecciated dolostone	Galena, sphalerite and pyrite (traces of chalcopyrite) in gangue of dolomite and calcite.
Shag	MVT	Zn, Pb (±Ag)	Stephen, Eldon and Waterfowl fms	Middle to Upper Cambrian	Dolostone	Sphalerite, galena, minor pyrite in a gangue of dolomite, quartz, and minor calcite.
Munroe	MVT	Zn	Palliser Fm; lower (Morro) mb	Upper Devonian	Dolostone with fenestral porosity (filled by white sparry dolomite), zebra-like texture, lesser breccia	Sphalerite, minor pyrite and galena in a gangue of dolomite; calcite and dolomite fill vugs.
Alpine	MVT	Zn	Palliser Fm; lower (Morro) mb	Upper Devonian	Dolostone	Sphalerite, minor pyrite and galena in a gangue of dolomite; calcite and dolomite fill vugs.
Boivin	MVT	Zn	Palliser Fm; lower (Morro) mb	Upper Devonian	Dolostone	Sphalerite, minor pyrite and galena in a gangue of dolomite; calcite and dolomite fill vugs.
Hawk Creek	MVT	Zn, Pb (±Ag, ±Au)	McKay Group	Upper Cambrian-Ordovician	Argillaceous limestone, argillite, dolomitic limestone.	Sphalerite, pyrite, galena (silver reported) in a gangue of calcite and dolomite.
Rock Canyon Creek	REE-F-Ba	REE-F-Ba	Cedared and Burnais fms	Middle Devonian	Dolostone, dolomitic limestone, carbonate breccia and laminated silty, calcareous gypsum.	Dolomite, fluorite, barite, pyrite, quartz, K-feldspar, calcite, REE-fluorocarbonates and REE-phosphates.
Oldman	MVT	Pb, Zn, Ag	Upper Palliser Fm	Upper Devonian	Dolostone, dolomitic limestone, limestone.	Galena, pyrite, and sphalerite in a gangue of calcite. Minor: dolomite, ankerite.

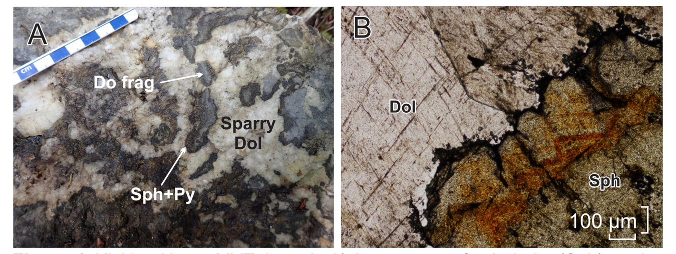

Figure 4. Kicking Horse MVT deposit. A) Aggregates of sphalerite (Sph)+pyrite (Py) in white sparry dolomite (Do) cement. B) Colloform sphalerite exhibiting colour zonation adjacent to white sparry dolomite; PPL = Plane-Polarized Light.

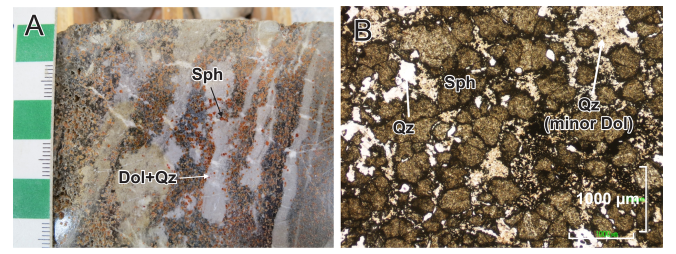

Figure 5. Shag MVT deposit. A) Sample of Red Bed showing displays alternating bands of white dolomite and quartz and darker dolostone rich in red sphalerite (Sph). B) The C-4 showing with intense replacement by granular sphalerite in a matrix of quartz and dolomite, with minor pyrite and galena (black); PPL.

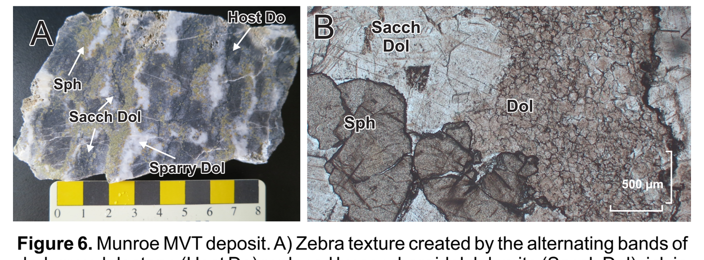

Figure 6. Munroe MVT deposit. A) Zebra texture created by the alternating bands of dark grey dolostone (Host Do) replaced by saccharoidal dolomite (Sacch Dol) rich in sphalerite (Sph), and white sparry dolomite lenses. B) Nonplanar or planar-e to planar-s dolomite (Dol), coarser-grained saccharoidal dolomite (Sacch Dol) and intergranular sphalerite (Sph); PPL.

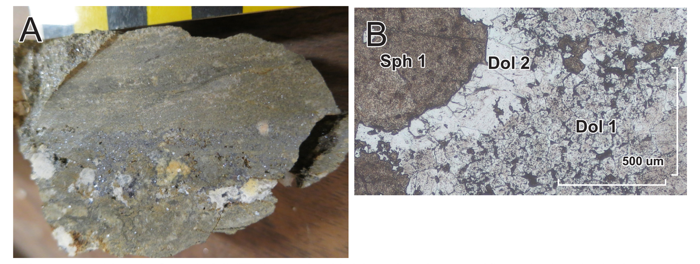

Figure 7. Hawk Creek MVT deposit. A) Massive layered/banded sphalerite and less pyrite, galena replacing argillites and argillaceous dolostone of the middle Cambrian McKay Group. B) Sphalerite 1 (Sph 1) surrounded by fine crystalline dolomite (Dol 1) and coarse-grained saddle dolomite (Dol 2); PPL.

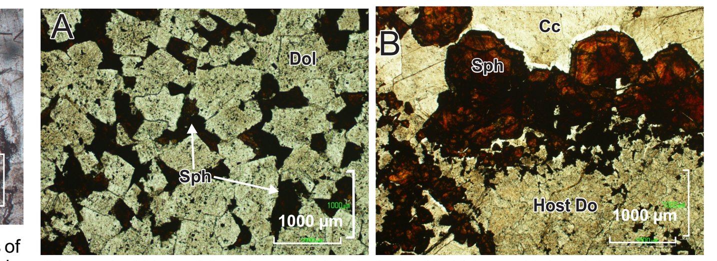

Figure 8. Oldman MVT deposit. A) Sphalerite (Sph) interstitial to dolomite (Dol); PPL. B) Colloform sphalerite (Sph) fills open spaces. Smaller grains are interstitial to or replace the dolomite (Host Do); PPL.

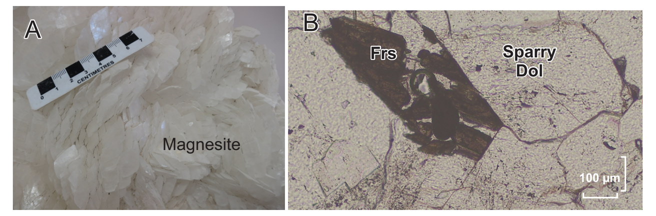

Figure 9. Mount Brussilof magnesite deposit (Baymag mine). A) Coarse-grained grey magnesite ore. B) Fersmite (Frs) crystal in sparry dolomite (Sparry Dol); PPL.

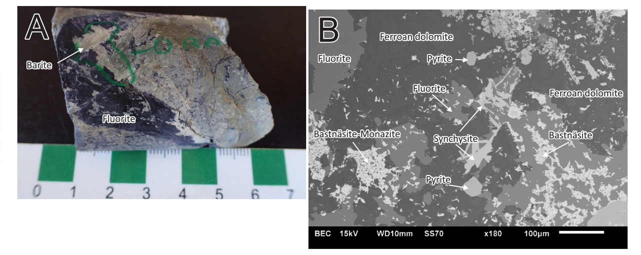

Figure 10. Rock Canyon Creek REE-F-Ba deposit. A) Large euhedral crystals of barite in purple fluorite vein cutting altered dolostone (DDH-09-01 at 38.7 m). B) Backscatter electron image of mineral assemblage from the REE-F-Ba mineralization.

Geochemistry and Fluid Inclusion Results

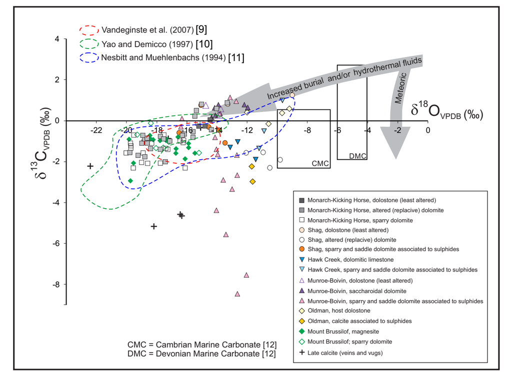

Figure 11. $\delta^{13}C_{VPDB}$ versus $\delta^{18}O_{VPDB}$ of host dolostone and hydrothermal dolomites associated with MVT and magnesite deposits. Hydrothermal dolomites associated with mineralization have lower $\delta^{18}O_{VPDB}$ values than their respective dolostone host rocks. Our data compare well with the hydrothermal dolomites of [9], [10] and [11]. The generalized trends for burial, hydrothermal and meteoric fluids of [13] are illustrated by arrows.

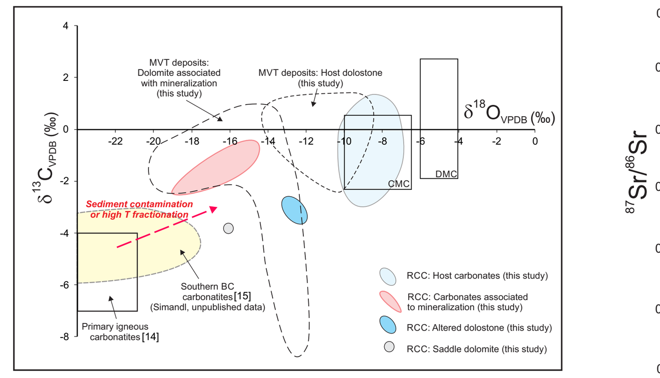

Figure 12. Plot of $\delta^{13}C_{VPDB}$ versus $\delta^{18}O_{VPDB}$. Values for dolomites associated with MVT, magnesite, and REE-F-Ba deposits are lower than respective host carbonate rocks. Dolomite associated with Rock Canyon Creek (RCC) REE-F-Ba mineralization has $\delta^{13}C_{VPDB}$ versus $\delta^{18}O_{VPDB}$ values similar to dolomite associated with MVT and magnesite deposits; these values plot outside the fields of southern British Columbia carbonatite (yellow) and primary igneous carbonatites (defined by [14]).

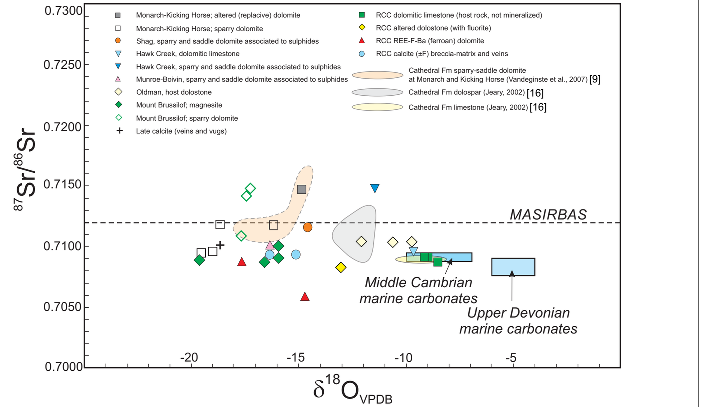

Figure 13. $\delta^{18}O_{VPDB}$ versus $^{87}Sr/^{86}Sr$ values for various carbonates associated with deposits of the southern Canadian Rocky Mountains. Middle Cambrian and Devonian marine carbonate values are from [12]. Maximum Sr isotope ratio of basin shale (MASIRBAS) is from [17]. $^{87}Sr/^{86}Sr$ values of MVT and magnesite hydrothermal dolomites are similar or higher than their host dolostone. However, Rock Canyon Creek dolomites have lower $^{87}Sr/^{86}Sr$ values than those from MVT and magnesite deposits.

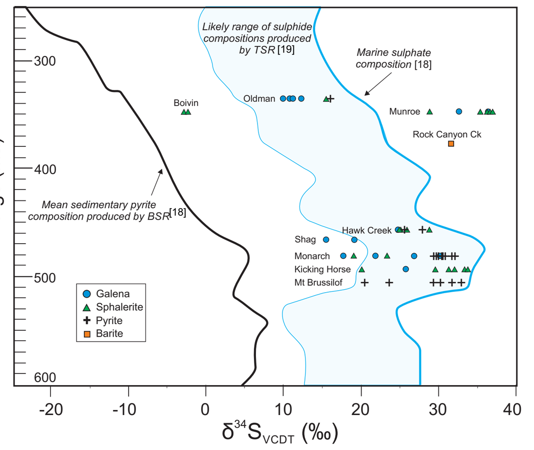

Figure 14. Sulphur isotope values of carbonate-hosted deposits in relation to age of host rocks. Sulphur in most MVT deposits is consistent with an origin from seawater sulphate, reduced by thermogenic sulphate reduction (TSR) and locally bacterogenic sulphate reduction (BSR) occurred. Modified from [20].

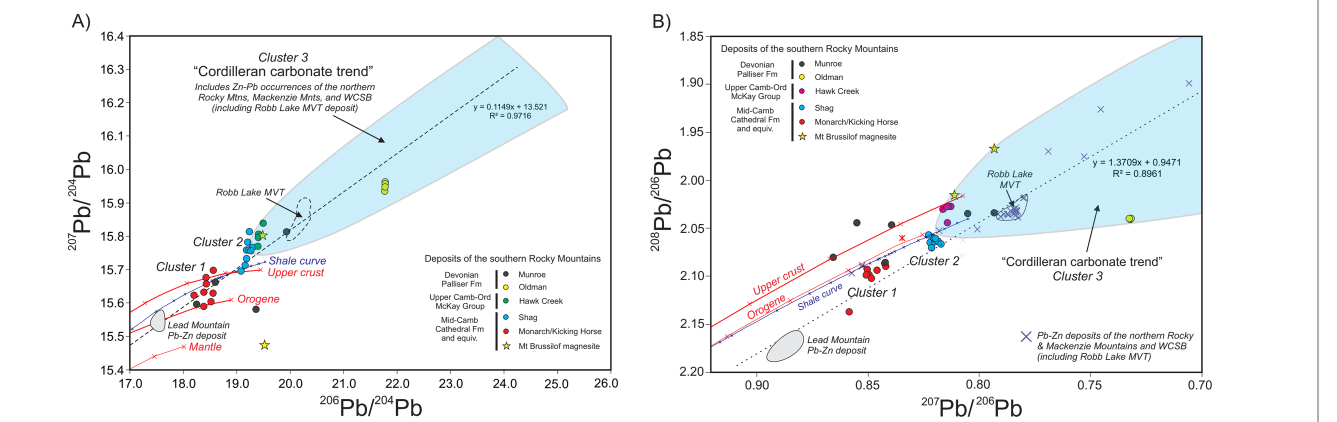

Figure 15. A) $^{207}Pb/^{204}Pb$ versus $^{206}Pb/^{204}Pb$; and B) $^{207}Pb/^{206}Pb$ versus $^{208}Pb/^{206}Pb$ of galena, pyrite, and sphalerite from carbonate-hosted deposits of the southern Rocky Mountains compared to the "Cordilleran carbonate trend", which includes Zn-Pb occurrences and deposits of the northern Rocky Mountains, Mackenzie Mountains, and Western Canada Sedimentary Basin (WCSB). The data form 3 clusters, each defined by specific deposits. Cluster 1, the least radiogenic group, is from the Monarch, Kicking Horse and Munroe deposits. Cluster 2 consists exclusively of samples from Shag deposits. Cluster 3, the most radiogenic group, consists of Hawk Creek, Mount Brussilof, Oldman, and Munroe deposits, which plot within the "Cordilleran-carbonate trend" defined by carbonate-hosted Zn-Pb deposits and occurrences of the northern Rocky Mountains, Mackenzie platform, and WCSB (cf. [21]). The dashed lines in A) and B) represent the trendline for all the data within the "Cordilleran carbonate trend". They intersect clusters 1 and 2, and a cluster of unradiogenic lead data from the Lead Mountain deposit, a vein- and fracture-controlled carbonate-hosted sulphide-barite deposits in the western Foreland Belt of the Rocky Mountains. This suggests that Pb signature of clusters 1, 2, and 3 represents mixtures of variably radiogenic end members.

Fluid Inclusions

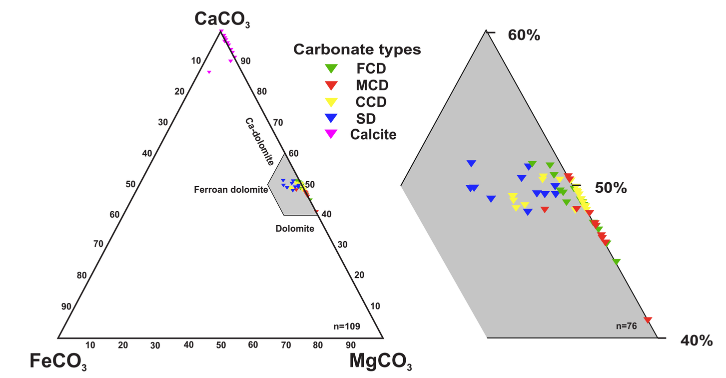

Figure 16. Ternary plots of $CaCO_3$-$FeCO_3$-$MgCO_3$ (in atomic %) for different dolomite types and calcite from different study areas. Dolomite is generally stoichiometric chemically, but ore-stage types (CCD and SD) are the most Fe-rich (up to 6 mol % $FeCO_3$). Data were collected using SEM-EDS analysis. Abbreviations: FCD = fine-grained crystalline dolostone (~host dolostone), MCD = medium-grained crystalline dolomite, CCD = coarse-grained crystalline dolomite, SD = saddle dolomite [22].

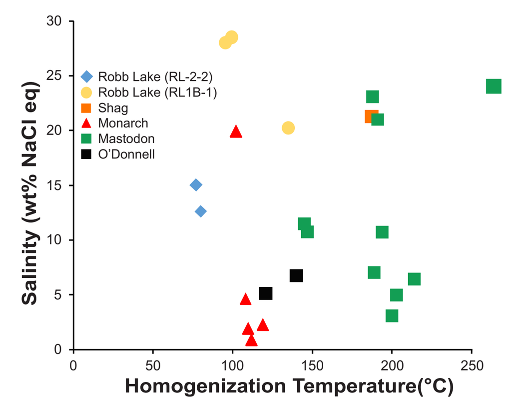

Figure 17. Homogenization temperature (Th) versus salinity (wt. % equiv. NaCl). The data indicate broad ranges of temperature (<80–200°C) and salinity (0.9–28 wt.%), even in some cases for single settings (e.g., Monarch 0.9–20.2 wt. %; Mastodon 3.1–23.1 wt. %). Mastodon and O'Donnell deposits are located in the Kootenay Arc of southern BC [22].

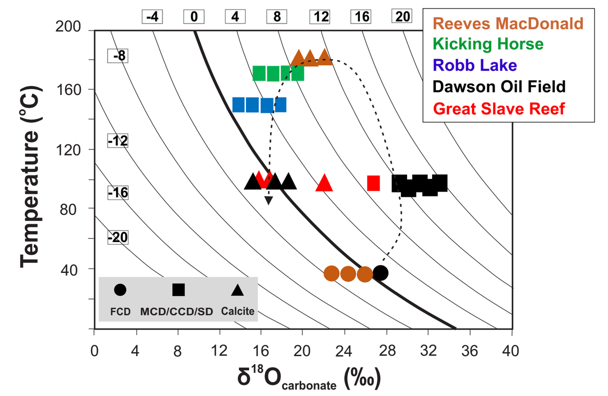

Figure 18. Plot of $\delta^{18}O_{SMOW}$ (‰) values for different carbonate types versus Temperature. The curved lines are $\delta^{18}O_{H2O}$ values of precipitating fluids calculated using the dolomite-H_2O fractionation equation of [22]. The dashed black line traces the idealized evolutionary trend of a fluid in a MVT setting [23]. Reeves MacDonald deposit is in the Kootenay Arc of southern BC, and Dawson Oil Field and Great Slave Reef are in the Western Canada Sedimentary Basin.

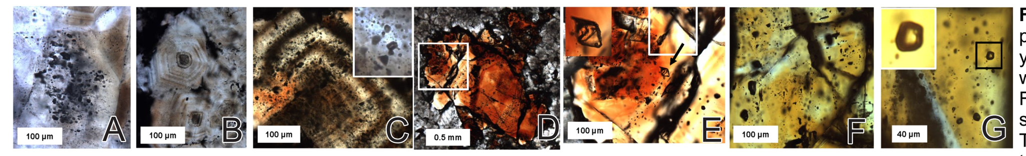

Figure 19. Fluid inclusions (FI) hosted in sphalerite. The inclusions are primary (P), pseudosecondary (PS) and secondary (S) and indeterminate (I) types. A) Kicking Horse: zoned, yellow to clear sphalerite with FI of P types. B) Monarch: zoned yellow to clear sphalerite inundated with opaque FI of P types. C) Monarch: clear to red zoned sphalerite inundated with irregular-shaped FI of P, S and I types. D) & E) Shag: zoned red to clear sphalerite with FI of P and S types. Image E shows an enlarged FI (black arrow) with low vapour phase relative to liquid (V:L ratio) and thus a low Th value (<80°). F) & G) Shag: clear to yellow, zoned sphalerite hosting small to large, equant FI of I type defining a 3D array. Most of the FI are opaque, but inset with outlined black box is a small vapour phase [22].

Ages

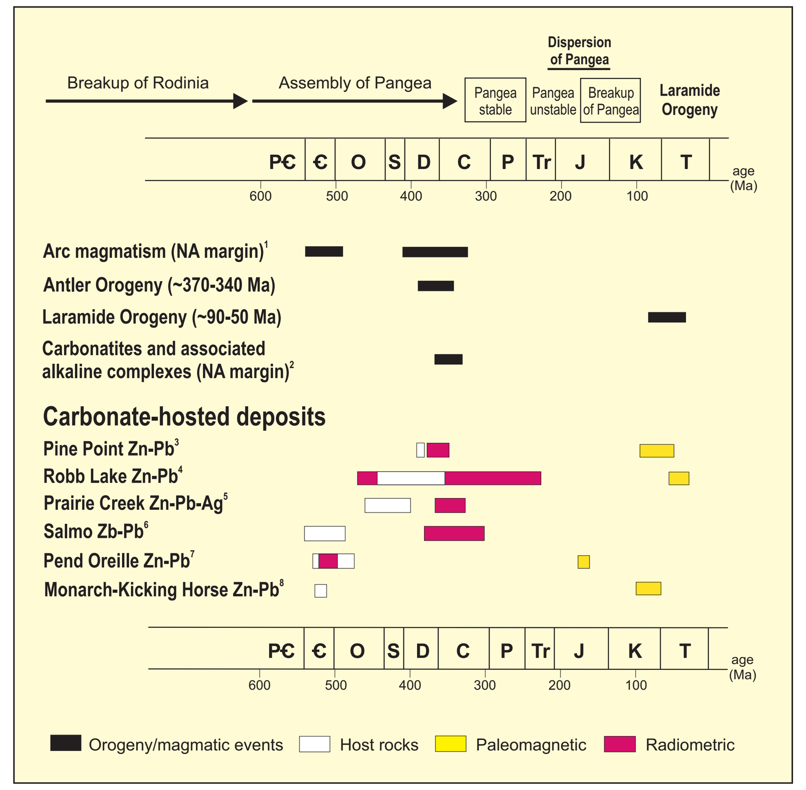

Figure 20. Summary of known radiometric and paleomagnetic ages of Zn-Pb carbonate-hosted mineralization and their host rocks. Figure modified from [24]. [1]Data from [25]; [2]Radiometric data from various sources and compiled by [26]. Abbreviation: NA – North America; [3]Radiometric data (Rb-Sr) from [27], paleomagnetic data from [28]; [4]Radiometric data (Rb-Sr) from [21], paleomagnetic data from [29]; [5]Radiometric data (Re-Os) from [30] and [31] (work in progress); [6]Radiometric data (Re-Os) from [30], [31] and [32]; [7]Paleomagnetic data from [33], radiometric data from [34]; [8]Paleomagnetic data from [35].

Conclusions

- Deposits covered by this study are hosted by shallow-water platform carbonate rocks of Ancestral North America (**Fig. 1**). They are located east of the Rocky Mountain trench along the projection of the Cathedral escarpment (**Fig. 2**). This escarpment coincides with structurally controlled facies transitions between platform carbonate rocks and deep-water basin rocks.
- Deposits are associated with syn- to post-depositional dolomitization represented by "replacive", sparry and saddle dolomites (**Fig. 4 to 10**). These dolomites resulted from hydrothermal fluid migration along fault systems and strata with enhanced porosity and permeability.
- The $\delta^{18}O_{VPDB}$ (-20.0 to -9.8‰) and $\delta^{13}C_{VPDB}$ (-8.6 to +1.1‰) values for "replacive", sparry, and saddle dolomites associated with MVT, magnesite, and REE-F-Ba deposits are lower than their respective host carbonate rocks ($\delta^{18}O_{VPDB}$= -15.2 to -7.1‰; $\delta^{13}C_{VPDB}$= -2.9 to +1.2‰), and they compare well with other hydrothermal dolomites in the RMFB **(Fig. 11, 12)**.
- The $\delta^{18}O_{VPDB}$ and $\delta^{13}C_{VPDB}$ values of hydrothermal dolomites at Rock Canyon Creek REE-F-Ba deposit are intermediate between values of carbonatites and host carbonate rocks (**Fig. 12**). Their $^{87}Sr/^{86}Sr$ values (0.70588 to 0.70873; **Fig. 13**) are similar or lower than their host carbonate rocks (0.70866 to 0.70903). This suggests that REE-F-Ba mineralization at Rock Canyon Creek may have formed from distal carbonatite-related fluids interacting with carbonate host rocks and mixing with ambient fluids.
- Sulphur isotope values of Sulphide minerals show large variations within a deposit (e.g. +20.5 to +32.9‰ at Mount Brussilof) and among different deposits (e.g. across all deposits, $\delta^{34}S_{VCDT}$ values range from -2.8% to +36.6%, n=53, with most values from +9.9 to +36.6‰, n=51). Reduced sulphur formation predominantly occurred through TSR of coeval seawater sulphate for most deposits (e.g. Kicking Horse, Monarch, and Hawk Creek). However, BSR also occurred locally (e.g. at Boivin; **Fig.14**).
- Lead isotopes suggest a mixing trend involving highly radiogenic and non-radiogenic end members (**Fig. 15**).
- Dolomite composition is typically stoichiometric; however, ore-stage varieties ("replacive", coarse-grained sparry and saddle dolomites) are enriched in Fe (up to 6 mol % $FeCO_3$; **Fig. 16**).
- The homogenization temperatures, measured from fluid inclusions trapped in sphalerite from the Rocky Mountains MVT deposits (~ 160−240ºC, pressure corrected to 1 kbar; **Figs. 17, 18, 19**), support a hydrothermal origin.
- Fluids responsible for "replacive", sparry and saddle dolomites associated with MVT and magnesite deposits were of hydrothermal origin, modified by interaction with siliclastic and carbonate rocks, and were expelled from deep burial settings by tectonic stresses, as exemplified by high temperatures (~ 160−240ºC), low $\delta^{18}O_{VPDB}$ values (-20.0 to -11.5‰), and high $^{87}Sr/^{86}Sr$ ratios (0.70879 to 0.71484).
- Mineralization occurred intermittently (in more than one stage) during the Paleozoic, i.e. middle to late Cambrian and Late Devonian to middle Carboniferous (**Fig. 20**).

TGI Ore Systems
Targeted Geoscience Initiative
Initiative géoscientifique ciblée

References: 1. Colpron, M., and Nelson, J.L., 2011; Yukon Geological Survey, www.geology.gov.yk.ca/bedrock_terrane.html, accessed December 2012; also BC Geological Survey, BC GeoFile 2011-11, http://www.empr.gov.bc.ca/Mining/Geoscience/PublicationsCatalogue/GeoFiles/Pages/2011-11.aspx. 2. Aitken, J.D., 1971; Bulletin of Canadian Petroleum Geology, v. 19, p. 557– 569. 3. Aitken, J.D., 1989; Bulletin of Canadian Petroleum Geology, v. 37, p. 316–333. 4. Katay, F., 2017; British Columbia Ministry of Energy and Mines, British Columbia Geological Survey, Information Circular 2017-1, p. 73–107. 5. Cui, Y., Miller, D., Nixon, G., and Nelson, J., 2015; British Columbia Ministry of Energy and Mines, British Columbia Geological Survey, Open File 2015-2. 6. Paradis, S., Simandl, G.J., Drage, N., D'Souza, R.J., Kontak, D.J., and Waller, Z., 2020; Geological Survey of Canada, Bulletin XXX, p. Y–Z. 7. Price, R.A. 1981; Geological Society of London, Special Publication No. 9, pp. 427–448. 8. McMechan, M.E., 2012; Canadian Journal of Earth Sciences, v. 49, no. 5, p. 693-708. 9. Vandeginste, V., Swennen, R., Gleeson, S.A., Ellam, R.M., Osadetz, K., and Roure, F., 2007; Mineralium Deposita, v. 42, p. 913–935. 10. Yao, Q. and Demicco, R.V., 1997; American Journal of Science, v. 297, p. 892–938. 11. Nesbitt, B.E. and Muehlenbachs, K., 1994; Geology, v. 22, p. 243–246. 12. Veizer, J., Ala, D., Azmy, K., Bruckschen, P., Buhl, D., Bruhn, F., Carden, G.A.F., Diener, A., Ebneth, S., Godderis, Y., Jasper, T., Korte, C., Pawellek, F., Podlaha, O.G., Strauss, H., 1999; Chemical Geology, v. 161, p. 59–88. 13. Choquette, P.W. and James, N.P., 1987; Geoscience Canada, v. 14, p. 3-35. 14. Taylor, H.P., Frechen, J., and Degens, E.T., 1967; Geochimica et Cosmochimica Acta, v. 31, p. 407–430. 15. Simandl, G.J., Petrus, J., Leybourne, M., and Paradis, S., 2018; Resources for Future Generations Resources for Future Generations 2018, Vancouver, British Columbia, June 16-21, 2018, Abstracts. 16. Jeary, V.A., 2002; M.Sc. thesis, University of Calgary, Calgary, Alberta, 250 p. 16. Machel, H.G. and Cavell, P.A., 1999; Bulletin of Canadian Petroleum Geology, v. 47, p. 510–533. 17. Machel and Cavell, 1999; Bulletin of Canadian Petroleum Geology, v. 47, p. 510-533. 18. Farquhar J., Wu, N.P., Canfield, D.E., and Oduro, H., 2010; Economic Geology, v. 105, p. 509–533. 19. Kiyosu, Y. and Krouse, H.R., 1990; Geochemical Journal, v. 24, p. 21–27. 20. Wilkinson, J.J., 2014; Geochemistry of Mineral Deposits: Treatise on Geochemistry (second edition), (ed.) S.D. Scott; Elsevier, v. 13, p. 219-249. 21. Nelson, J.L., Paradis, S., Christensen, J., and Gabites, J., 2002; Economic Geology, v. 97, p. 1013–1036. 22. Kontak, D.J, Paradis, S., Waller, Z., and Fayek, M., 2020; Geological Survey of Canada, Bulletin XXX, p. Y–Z. 23. Horita, J.,2014; Geochimica et Cosmochimica Acta, v. 129, p. 111-124. 24. Leach, D.L., Bradley, D., Lewchuk, M.T., Symons, D.T.A., de Marsily, G., and Brannon, J., 2001; Mineralium Deposita v. 36, p. 711–740. 25. Nelson, J.L., Colpron, M., Piercey, S.J., Dusel-Bacon, C., Murphy, D.C., and Roots, C.F., 2006; Geological Association of Canada, Special Paper 45, p. 323-360. 26. Millonig, L.J., Gerdes, A. and Groat, L.A., 2012; Lithos, v. 152, p. 202–217. 27. Nakai, S.I., Halliday, A N., Kesler, S.E., Jones, H.D., Kyle, J.R., and Lane, T.E., 1993; Geochimica et Cosmochimica Acta, v. 57, p. 417-427. 28. Symons, D.T.A., Pan, H., Sangster, D.F., and Jowett, E.C., 1993; Canadian Journal of Earth Sciences, v. 30, p. 1028-1036. 29. Smethurst, M.T., Sangster, D.F., Symons, D.T.A., and Lewchuk, M.T., 1999; Bulletin of Canadian Petroleum Geology, v. 47, p. 548-555. 30. Hnatyshin, D. 2018; PhD thesis, University of Alberta, Edmonton, Alberta, 306 p. 31. Hnatyshin, D. van Acken, D., Paradis, S., Creaser, C.R. (in preparation). Submitted to Economic Geology. 32. Paradis, S., Gleeson, S., and Magnall, J., 2014; Prospectors and Developers Association of Canada (PDAC), Zinc session. Abstracts with Programs. 33. Pannalal, S.J., Symons, D.T.A., and Leach, D.L., 2007; Canadian Journal of Earth Sciences, v. 44, p. 1661–1673. 34. Paradis, S., Hnatyshin, D., Simandl, G.J., and Creaser, R.A., 2020; Economic Geology, in press. 35. Symons, D.T.A., Lewchuk, M.T., and Sangster, D.F., 1998; Economic Geology, v. 93, p. 68–83.

Acknowledgments:
This study benefited from the assistance and collaboration of Fiona Katay (British Columbia Ministry of Energy and Mines, Regional Geologist based in Cranbrook), and field assistant Michaella Yakimoski (student at University of Victoria). We thank David Pighin and Chris Graf for their perspectives on the geology of the Rocky Mountains and providing samples. Baymag Inc. kindly provided access to the Mount Brussilof mine. Special thank you extends to Ian Knuckey, mine manager, and Alex Hogg and Brody Myers, mine geologists. Wylee Fitz-Gerald helped with setting up and editing the final version of this document.